frontiers in Earth Science

ORIGINAL RESEARCH
published: 23 December 2021
doi: 10.3389/feart.2021.741287

Upward Magma Migration Within the Multi-Level Plumbing System of the Changbaishan Volcano (China/North Korea) Revealed by the Modeling of 2018–2020 SAR Data

Elisa Trasatti[1], *Cristiano Tolomei*[1], *Lianhuan Wei*[2]* *and Guido Ventura*[1,3]

[1]*Istituto Nazionale di Geofisica e Vulcanologia, Roma, Italy,* [2]*School of Resources and Civil Engineering, Northeastern University, Shenyang, China,* [3]*Istituto per Lo Studio Degli Impatti Antropici e Sostenibilità in Ambiente Marino (IAS), Consiglio Nazionale Delle Ricerche, Capo Granitola (TP), Italy*

Changbaishan volcano (China/North Korea border) was responsible for the largest eruption of the first Millennium in 946 CE and is characterized by a multi-level plumbing system. It last erupted in 1903 and presently consists of a cone with summit caldera. An unrest episode occurred between 2002 and 2006, followed by subsidence. Here, we analyze the Changbaishan 2018–2020 deformations by using remote sensing data, detecting an up to 20 mm/yr, NW-SE elongated, Line of Sight movement of its southeastern flank and a –20 mm/yr Line of Sight movement of the southwestern flank. This reveals an unrest occurring during 2018–2020. Modeling results suggest that three active sources are responsible for the observed ground velocities: a deep tabular deflating source, a shallower inflating NW-SE elongated spheroid source, and a NW-SE striking dip-slip fault. The depth and geometry of the inferred sources are consistent with independent petrological and geophysical data. Our results reveal an upward magma migration from 14 to 7.7 km. The modeling of the leveling data of the 2002–2005 uplift and 2009–2011 subsidence depicts sources consistent with the 2018–2020 active system retrieved. The past uplift is interpreted as related to pressurization of the upper portion of the spheroid magma chamber, whereas the subsidence is consistent with the crystallization of its floor, this latter reactivated in 2018–2020. Therefore, Changbaishan is affected by an active magma recharge reactivating a NW-SE trending fault system. Satellite data analysis is a key tool to unravel the magma dynamics at poorly monitored and cross-border volcanoes.

Keywords: active magma recharge, plumbing system, changbaishan volcano, InSAR, deformation modeling

OPEN ACCESS

Edited by:
Vincent Drouin,
Icelandic Meteorological Office, Iceland

Reviewed by:
Olivier Galland,
University of Oslo, Norway
Yosuke Aoki,
The University of Tokyo, Japan

***Correspondence:**
Lianhuan Wei
weilianhuan@mail.neu.edu.cn

Specialty section:
This article was submitted to Volcanology, a section of the journal Frontiers in Earth Science

Received: *14 July 2021*
Accepted: *06 December 2021*
Published: *23 December 2021*

Citation:
Trasatti E, Tolomei C, Wei L and Ventura G (2021) Upward Magma Migration Within the Multi-Level Plumbing System of the Changbaishan Volcano (China/North Korea) Revealed by the Modeling of 2018–2020 SAR Data. Front. Earth Sci. 9:741287. doi: 10.3389/feart.2021.741287

INTRODUCTION

Volcanic unrest is generally associated with deformations, seismicity, and variations in the gas/water geochemistry testifying magma accumulation or migration processes or gas ascent and expansion or pressurization (Newhall and Dzurisin, 1988; Acocella et al., 2015). Volcanoes with a closed conduit may be restless for decades or centuries without eruptions or with eruptions separated by long periods. Seismicity, gas discharge and alternate periods of uplift and subsidence usually indicate repeated intrusions of magma or gas pressurization at depth (e.g., Acocella et al., 2015); Campi

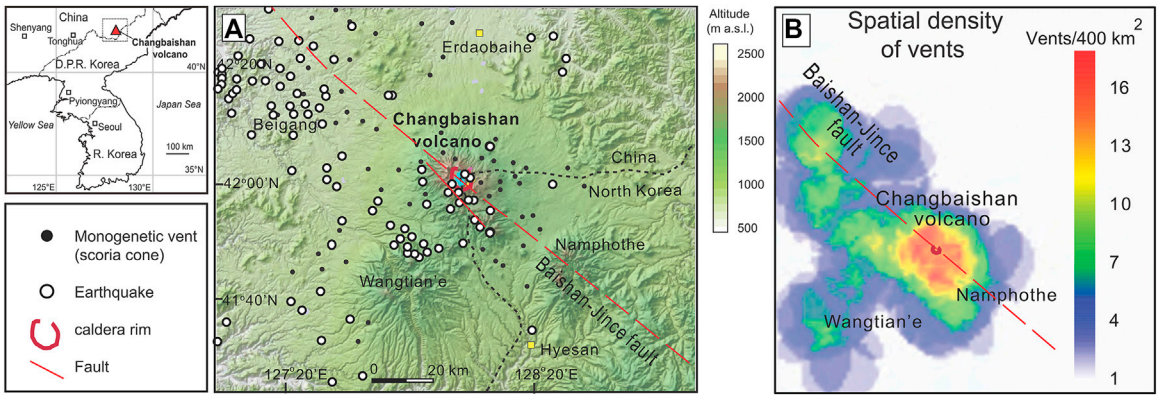

FIGURE 1 | Location map of the Changbaishan volcano (inset). **(A)** Simplified map of the main tectonic structures, earthquakes and vents in the Changbaishan area. The main structures and volcanic vent location are from Liu et al. (2004) and Zhang et al. (2018). Epicenters refer to earthquakes located by permanent seismic networks in the time interval 1977–2018 with M_L between 0.8 and 4.4 (redrawn from Pan et al., 2021). **(B)** Spatial density of vents, mainly scoria cones, in the Changbaishan area.

Flegrei caldera, Italy (Trasatti et al., 2015), Yellowstone, USA (Chang et al., 2010), Santorini, Greece (Papageorgiou et al., 2019), Taupo, New Zealand, (Hamling et al., 2016), are worldwide examples of such behavior. In addition, multiple phases of uplift may reflect more complex processes. These include magma chamber volume reduction and dilation of an overlying dike, as observed during the Hekla (Iceland) 2000 eruption (Sturkell et al., 2013), or the coeval processes of volume dilatation by degassing and magma contraction due to cooling (Caricchi et al., 2014). Therefore, the interpretation of monitoring signals may be not unequivocal also because 1) some unrest is accompanied by deformations without seismicity or changes in gas geochemistry (Phillipson et al., 2013), and 2) the plumbing system of many volcanoes is poorly known. This latter remark is particularly true for volcanoes characterized by a set of crystal-to melt-rich reservoirs located at different depths (Kennedy et al., 2018). As a result, the knowledge of the complex plumbing system of volcanoes is of primary importance to evaluate the volcano dynamics and assess the hazard. Changbaishan volcano (China/North Korea) (**Figure 1**) is characterized by a multi-level plumbing system consisting of reservoirs located at different depth and a shallower hydrothermal system (Zhang et al., 2015; Zhang et al., 2018; Yi et al., 2021).

Here, we analyze satellite images from the ALOS-2 platform acquired between November 2018 and October 2020 on Changbaishan, which last erupted in 1903 and underwent an unrest episode in 2002–2006. The volcano is characterized by a summit caldera filled by a lake and it is considered the most dangerous volcano in China and surrounding countries (Russia, North and South Korea) because it was responsible for the largest eruption of the first millennium on Earth, the magnitude $M = 7.2$, 946 CE "Millennium" eruption (Horn and Schmincke, 2000; Iacovino et al., 2016; Yi et al., 2021), whose products have been found in Russia, Japan, China Sea, Korean peninsula, and Greenland (Sun et al., 2014). Between 2002 and 2006, Changbaishan experienced an increase of seismicity, changes in the gas composition, and deformations (uplift) (Xu et al., 2012). This unrest episode was followed by a subsidence phase of lower amount during which only part of the uplift has been recovered. Our 2018–2020 multitemporal InSAR (Interferometric Synthetic Aperture Radar) analysis of ALOS-2 data records a new episode of inflation of the volcano mainly affecting its southeastern, North Korean sector. We show that the recorded inflation is not compatible with a volume change within a single source and requires a complex geometry suggesting a vertically extended plumbing system with mass transfer from deeper to shallower levels and the activation of a fault. Also, we model past deformation phases such as the 2002–2006 unrest and 2009–2011 subsidence providing a comprehensive view of the processes occurring in the Changbaishan plumbing system. We discuss our results considering the available geophysical and petrological data and we document that the volcano is in unrest with obvious implications for the volcanic hazard assessment at the China/North Korea boundary.

GEOLOGICAL AND GEOPHYSICAL SETTING

Eruptive History, Tectonics, and Recent Dynamics

Changbaishan intraplate volcano (2,774 m a.s.l., also known as Paektu, Baekdu, Tianchi; **Figure 1A**) is located at the China/North Korea boundary above the 500–600 km deep stagnant portion of the Pacific slab (Zhao, 2021). The volcano is affected by a summit caldera depression with a diameter of about 5 km filled by a lake, and its activity developed in three main stages (Zhang et al., 2018): a shield-forming stage (5.02–1.05 Ma), a cone-construction stage (1.37–0.01 Ma and mostly<1 Ma), and the more recent, caldera-forming stage (0.01 Ma to 1903 CE). This last stage produced trachytic-comenditic pumices during Plinian eruptions. The 4.77 Ma to 1.88 Ma old central volcanoes Wangtian'e and Namphothe are located about 40 km

southwest and southeast of Changbaishan, respectively. The basement of Changbaishan is constituted by the Gaima basalt plateau and the underlying crystalline and metamorphic rocks. The Gaima plateau and the Chagbaishan flanks are characterized by numerous monogenetic scoria cones roughly aligned along a NW-SE direction (Zhang et al., 2018; **Figures 1A,B**). This is also the strike of the active Baishan-Jince fault, the main structural discontinuity affecting the basement and Changbaishan edifice, and along which crustal earthquakes and monogenetic cones align (Liu et al., 2004; **Figures 1A,B**). The Changbaishan morphology consists of a slightly NW-SE elongated cone with a sub-circular caldera mainly formed during the M 7.2, "Millennium" eruption (ME) in 946 ± 20 CE (**Figure 1**) (Zhang et al., 2018). A NW-SE striking, SE dipping fault affects the western slope of the cone (Liu et al., 2004; **Figure 1**). Except for the earthquakes recorded during the 2002–2006 unrest, which concentrated in the Changbaishan caldera, the 1977–2018 events roughly align along this fault (**Figure 1A**). The above summarized structural, geophysical, and morphological data coherently indicate that the volcano formed on a NW-SE weakness zone possibly controlled by the Baishan-Jince regional fault system, which extends from North Korea to China. Changbaishan represents one of the most dangerous Eastern Asia volcanoes because of its 'Millennium' eruption (ME), which emitted about 96 ± 19 km^3 of pyroclastics and whose gas emissions had a global impact on climate (Horn and Schmincke, 2000; Iacovino et al., 2016; Yi et al., 2021). The 2002–2006 unrest characterized by deformations, earthquakes including low-frequency events, and changes in volcanic gas geochemistry (Xu et al., 2012). CO_2-rich degassing areas and hot water are widespread in the Changbaishan area with CO_2 discharge average values of 1.8×10^5 t/yr (Zhang et al., 2015). The $^3He/^4He$ of the emitted gas (Ra = 6.6 in 2006) and the B isotopic values suggest that the Changbaishan fluids are released by the asthenospheric mantle (Xu et al., 2012) metasomatized by recycled carbonates and organic metasediments of the Pacific stagnant slab (Zhang et al., 2015).

The Plumbing System

Thermobarometry petrological data indicate that the plumbing system consists of sill-like reservoirs located at different depths (Lee et al., 2021; Yi et al., 2021). Seismological, resistivity and gravity data (Choi et al., 2013; Qiu et al., 2014; Hammond et al., 2020) evidence the possible occurrence of melts between 4 and 8 km depth while the hydrothermal system is located at about 3 km depth (Liu et al., 2021). Petrological studies on the evolution of the Changbaishan magmatism based on clinopyroxene thermobarometers (Lee et al., 2021) indicate a large, sill-like reservoir located between 10 and 13 km depth, while fluid inclusion studies (Andreeva et al., 2018) confirm this deep reservoir and evidence, according to the previously reported geophysical data, two smaller and shallower reservoirs at 7–8 km depth and at 3.5–5 km depth. During the 2002–2006 unrest, the hypocentral depth of earthquakes ranged between 12 km and the surface with most events concentrated in the upper 4–5 km of the crust below the caldera (Liu et al., 2021). A strong reduction in the number of earthquakes occurred in the range 5–7 km and 9–12 km suggesting partly molten zones within the present-day plumbing system.

Deformation Pattern and Seismicity

GNSS, InSAR and leveling data do not record significant deformations in the 1992–98 period, whereas a 6.5 cm maximum uplift has been detected during the unrest from 2002 to 2006 (Ji et al., 2021). This uplift was followed by a subsidence between 2008 and 2011. By using GPS and levelling data and by applying a Mogi-like source, Xu et al. (2012) suggest that the depth of the 2002–2006 inflation was at 6 km, whereas Zhu et al. (2008) propose a depth of 9.2 km. However, Ji et al. (2021) remark that the low spatial resolutions and geographic distribution of the geodetic sites do not allow to better constrain the source of the 2002–2006 uplift. This issue was partly overcome by InSAR data, whose larger spatial coverage constrains a source located at about 9 km depth for the 2002–2006 unrest (Ji et al., 2013). Chen et al. (2008) analyze GPS, levelling, ENVISAT SAR and JERS-1 SAR data collected in 2002 and 2003 and conclude that the deformation field is consistent with two Mogi-type pressure sources: a deeper source at 7.9 km depth located below the Changbaishan caldera and a shallower one at 5.5 km depth located about 40 km southeast of the caldera in North Korea below the Namphothe volcano (**Figure 1**). These two sources are connected by the Baishan-Jince regional fault system. The post-unrest subsidence and the more recent dynamics of Chagbaishan are poorly known, lacking specific studies and available data. The only available data concern the seismicity (Pan et al., 2021); these data show that after 2002–2005, when an average of 500 events/yr with M_{Lmax} = 4.4 was detected, the seismicity sharply decreased to 30 events/year with M_{Lmax} = 2.8 between 2010 and 2018.

MULTI-TEMPORAL INSAR DATA ANALYSIS

Methods

The Interferometric Synthetic Aperture Radar (InSAR) technique allows the estimation of ground motion along the sensor Line-Of-Sight (LOS) direction. Traditional differential InSAR (DInSAR) consists of a differential interferogram between two co-registered SAR scenes acquired at different times over the same area, also considering a digital elevation model (DEM). The main limitations are due to geometrical-temporal decorrelation and atmospheric artifacts (e.g., Peltzer and Rosen, 1995). Targeting at more precise deformation monitoring, several multi-temporal InSAR (MTI) techniques have been proposed in the last decades, which exploit the redundancy offered by hundreds of image pairs to reduce the above-mentioned limitations (e.g., Ferretti et al., 2001; Berardino et al., 2002). The outcomes of MTI consist of a mean ground velocity map and the relative displacement time-series temporally referred to the first acquisition date of the image stack, and spatially referred to a stable reference point or area within the radar coverage.

One of the most adopted MTI algorithms is the Persistent Scatterers (PS) InSAR approach that is a proven differential interferometric technique which involves processing of multitemporal SAR data to identify persistently scattering ground features and their motion rates with millimeter precision (Ferretti et al., 2001). PS concept is based on finding permanent scatterers showing phase stability over a long period of time and aims to measure accurate surface movements. The advantage of such a technique is that it overcomes geometrical and temporal decorrelation issues in urban and rocky areas by using a large amount of radar images. The PS analysis starts with a linearly independent set of interferometric combinations with respect to the same master scene. After removal of the topographic phase using the simulated phase relative to a DEM, the geocoded pixels are further investigated based on their phase stability. Afterwards, PS candidates with stable phases are selected with a given threshold. To account for residual orbit errors, phase ramps can be calculated and removed from the interferograms using a set of ground control points. Finally, atmospheric effects can affect the remaining phase of the interferograms, so a double spatio-temporal filtering of the resulting time series is performed to separate the deformation from the atmospheric signals.

Due to the problem of heavy vegetation coverage, rugged topography, long time snow coverage (from October to May) and cloud coverage of the study area, the C-band (ENVISAT and Sentinel-1) SAR images collected by European Space Agency (ESA) suffer from extremely low coherence. On the contrary, the L-band ALOS-2 data allows to overcome such issues providing sufficient coherence and spatial density of PS points. Therefore, we process 19 ALOS-2 images (path 131, frame 830) from ascending orbit in the StripMap acquisition mode, provided by the Japanese Aerospatial Agency (JAXA). The incidence angle is 40.58° and the temporal spanning is between 20th November 2018 and 20th October 2020.The multi-temporal algorithm named Persistent Scatterers was adopted with the ENVI SARscape software (L3HarrisTM, https://www.l3harris.com/). Also, the April 9, 2019 acquisition is selected as master image (**Supplementary Figure S1**). The Shuttle Radar Topography Mission (SRTM) (Farr et al., 2007) with 1 arc-second (~30 m) pixel size DEM is used to remove the topographic phase contribution. Due to cloud coverage and rugged topography of Changbaishan area, the tropospheric phase error, which includes vertical stratification and turbulence, could affect the accuracy of deformation estimation (Parker et al., 2015). Here, the vertical stratification is removed using the SRTM DEM. For the removal of tropospheric turbulence, both a low-pass filtering of 1,200 m and a high-pass one of 365 days are performed. Finally, a ground pixel of 30 m is considered during the geocoding step. Snow coverage and dense vegetation are both important factors of coherence loss in multi-temporal InSAR. However, L-band SAR images, such as the ALOS-2 ones, have the characteristic to penetrate sparse vegetation and snow coverage. There are only 4 months (from June to September) without snow coverage on the Changbaishan volcano summit. Also, by comparing the coherence with the land cover (Ji et al., 2010), dense vegetation (e.g., forest, mixture of more forest and less soil) is the main reason for coherence loss in Changbaishan area. A coherence threshold of 0.8 is chosen to select the final set of PS, and areas around the caldera provide a sufficient amount of PS points.

RESULTS

The retrieved mean velocity from ALOS-2 data exhibits several features (**Figure 2**). There is a wide, elongated area showing positive velocities up to 20 mm/yr. The northern tip of this area includes the Changbaishan caldera and extends south-eastwards in the North Korean sector of the volcanic cone. As second evidence of the InSAR results, the southwestern flank of the volcano shows negative mean LOS velocities reaching −20 mm/yr. In particular, there is an abrupt change in the mean velocities from negative values, below about 2000 m a.s.l. of altitude, to positive values at higher altitudes, on the upper southeastern flank of the volcano. This change is NW-SW trending and overlaps the trace of the NW-SE striking fault affecting the southwestern flank of Changbaishan (**Figure 1**; Liu et al., 2004). As a third feature of the mean velocity results, there are far field negative zones located north and east of Changbaishan, mainly in the plain surrounding the cone. Here, the velocities range from −3 to −10 mm/yr.

MODELING OF THE DEFORMATION

The 2018–2020 ground velocity map obtained by InSAR analysis shows a complex pattern, not interpretable by the activity of a single Mogi-like source that would provide the well-known bell-shaped vertical pattern. Here, the modeling is designed based on the features identified in the velocity map and by geophysical and volcanological independent information of the volcanic area discussed above.

We adopt three different sources consistent with the vertically extended plumbing system and an active tectonic structure. A spheroidal nearly horizontal pressurized source accounts for the NW-SE oriented area of positive LOS velocities. This pattern is clearly confined to the west, and we assume the action of a NW-SE striking fault, dipping to the SW (**Figure 1**), assumed to move with a dip-slip mechanism according to morphological evidence (Liu et al., 2004) and the retrieved displacement pattern. Also, we consider a partially deep melt zone consistent with evidence from seismological and petrological studies (Choi et al., 2013; Andreeva et al., 2018). The volume decrease within this deep tabular reservoir contributes to the far field negative LOS velocities observed to the north and east.

2018–2020 InSAR Data Inversion

Initially, InSAR data have been downsampled considering a varying length increasing from 250 m close to the crater, to 500 m and up to 1,500 m in the far-field. The inversion of geodetic data is performed by a Bayesian global optimization tool. The Bayesian inference is one of the inversion options available in VSM—Volcano and Seismic source Modelling

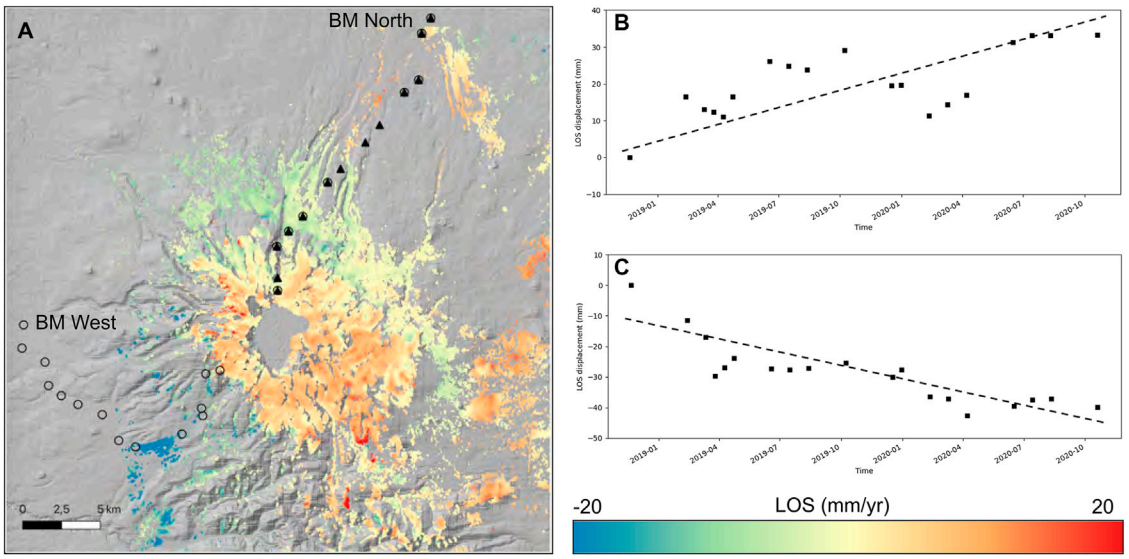

FIGURE 2 | (A) Mean velocity map from InSAR (PS) processing of ALOS-2 data. The open circles are the benchmarks from the western and northern leveling routes measured during the 2009–2011 campaigns, the full triangles are the northern leveling benchmarks measured during the 2002–2005 campaigns. **(B,C)** Displacement time series in the areas of maximum deformation, positive LOS velocity pixel **(B)**, negative LOS velocities pixel **(C)**.

(Trasatti, 2019). VSM implements the most common deformation sources that may be combined, and the most common geodetic data-types (SAR, GNSS, leveling, etc.). The Bayesian optimizer samples the parameters space using a Monte Carlo setting and combines the a-priori information with the likelihood computations to obtain posterior probability density functions of the parameters (Mosegaard and Tarantola, 1995). The Changbaishan active sources are represented by the above defined plumbing system and active fault. The medium is assumed as homogeneous and isotropic with shear modulus μ = 30 GPa and Poisson ratio equal 0.25. Inelastic rheology is likely to take place at volcanoes; however due to the limited time window covered and the seismicity located in the upper crust below the volcano, we consider mean ground velocities and linear elasticity of the medium. After several attempts, we choose an inflating spheroidal source (Yang et al., 1988) instead of an isotropic point-source (Mogi, 1958) to reproduce the NW-SE elongated high positive LOS velocities. The assumed source is a NW-SE elongated horizontal spheroid with fixed strike N140°E and axes proportion 1:3. A second volumetric source characterized by negative volume variation is fixed at 14 km b.s.L. and it is represented by a square tabular reservoir undergoing negative perpendicular displacement (Okada, 1985). This deep reservoir is centered below the caldera. Then, a NW-SE dip-slip fault is considered (Okada, 1985), whose characteristics such as strike, dip, position, and extension are based on previous studies (**Figure 1**) and on the InSAR velocity pattern depicted in **Figure 2**. We are aware that different settings of the active sources may be equally consistent with data. Our model configuration of the plumbing system is compatible with data and, at the same time, limits the number of unknowns.

The mean parameters resulting from the inversion of the InSAR data are reported in **Supplementary Table S1**, while the synthetic velocities and their comparison with data are reported in **Figure 3**. The 1D and 2D posterior probability density functions of the inverted parameters are reported in the **Supplementary Figure S2**, along with the samples collected during the random walks (**Supplementary Figure S3**). Comparisons with subsampled data are reported in **Supplementary Figure S4**.

The spheroid lays SE of the caldera, at 8.7 km below the reference height here fixed at 1,000 m, therefore we consider it to be located at about 7.7 km b.s.L. The reference height is usually chosen as the average elevation of the used data in case of remarkable topography (Bonaccorso et al., 2005). The volume variation estimated for the inflating spheroid is 7.3 ± 2.4 106 m^3/yr, while the retrieved finite volume amounts to about 300 km^3. The volume variation of the deeper tabular reservoir (laying 14 km b.s.L.) is -14 ± 4 106 m^3/yr. The amount of contraction of the deep reservoir in terms of its decreasing annual volume is almost twice the inflation of the shallower inflating source.

Figure 3 reports the results of the modeling and comparisons with data. In particular, the NW-SE trending main uplift area is reproduced by the spheroidal source. Also, the presence of the active dip-slip fault inhibits inflation in the western sector of Changbaishan volcano, as shown in **Figure 3B**. The far-field displacements are also reproduced on average. **Figure 3C** shows residuals, i.e., the difference between data and modelled LOS displacements. Pixels in white are within the uncertainty associated with InSAR data, here fixed at 4 mm/yr according to, e.g., Casu et al. (2006). **Figures 3D,E** shows the comparison between data and model along the NW-SE and SW-NE profiles depicted in **Figure 3A**. The ALOS-2 velocities are quite scattered, and the model reproduces them on average. The negative to positive velocities along the NW-SE profile are reproduced by the combined action of the shallow inflating source and the deep

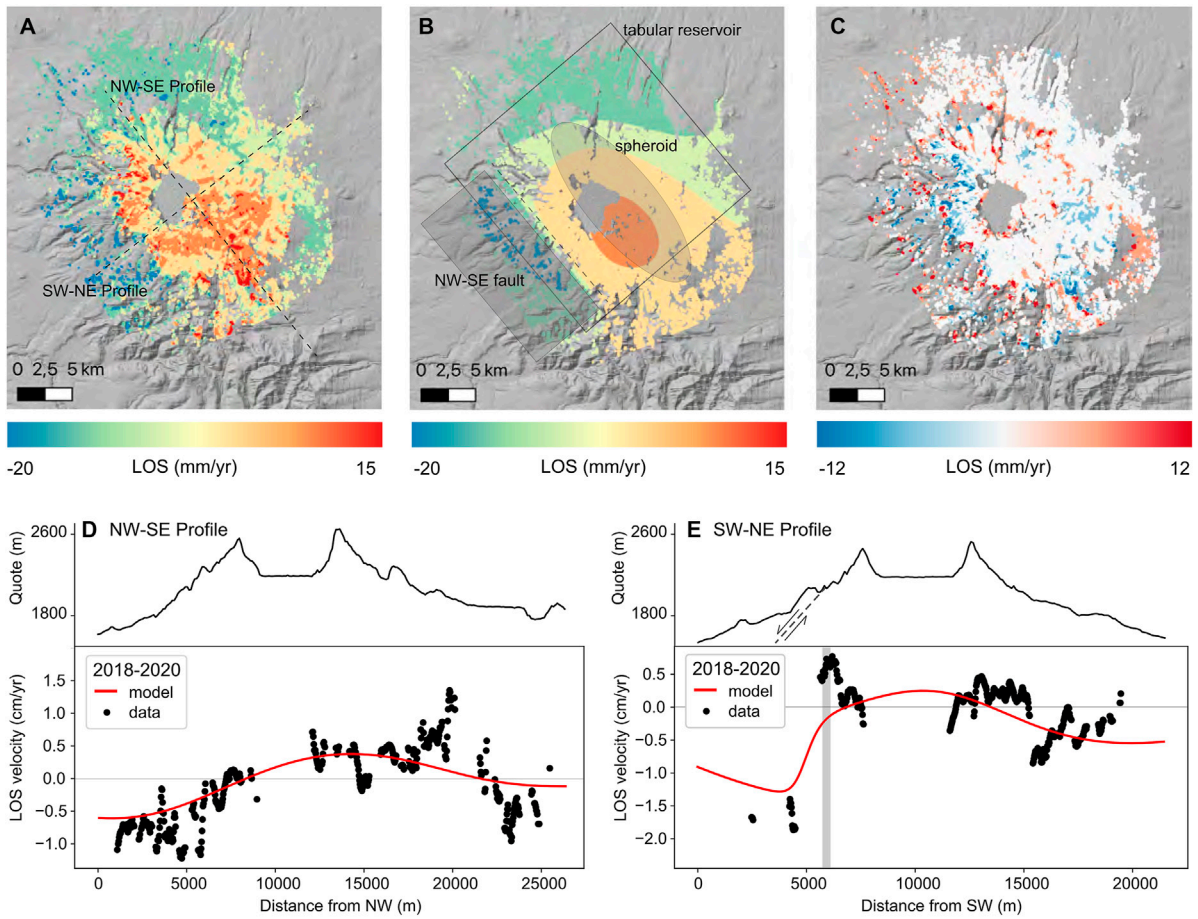

FIGURE 3 | Comparison between **(A)** InSAR ALOS-2 data and **(B)** LOS displacements generated by the mean model obtained by non-linear inversion. The surface projection of the spheroid, the tabular reservoir and the NW-SE fault are also reported in shaded grey. Residuals, i.e. difference between observed data (**Figure 2**) and modelled data are reported in **(C, D)** NW-SE and **(E)** SW-NE profiles as reported in **Figure 2**, with LOS data from ALOS-2 (black dots) and model (red line). The grey vertical bar is the approximate location of the NW-SE trending fault trace located in the western flank of the volcano. On the top is reported the topographic relief along the profiles. The dashed line is the NW-SE fault seen in a section across the volcano edifice.

tabular deflating source. The peaks on the SE are due to residual tropospheric turbulence and cannot be reproduced by the analytical models. On the other hand, the SW-NE profile clearly highlights a jump in the velocities while crossing the NW-SE trending fault (grey vertical line in **Figure 3E**). The negative velocities on the western side of the volcano, west of the fault, and the short-wavelength positive velocities moving towards the caldera are simulated by the dip-slip mechanism combined with the spheroid inflation. We exclude that the deformation pattern depicted in **Figure 3E** (SW-NE profile) could reflect magma related dynamics including cooling and/or degassing because there is no evidence of magma reservoirs in the western sector of the volcano (Ji et al., 2010, 2013; Choi et al., 2013; Hammond et al., 2020). The deformation field is consistent with movements along an outcropping fault. This fault may move in response to gravity-driven processes on the western flank of the volcano. This is supported by the steep topography (**Figure 3E**) and by the transition from hard rock (lava flows and domes) to partly loose material (pyroclastics). Finally, data close to the caldera rim show local minima/maxima and may be affected by residual geometrical artifacts in the InSAR analysis, due to the steep slopes and/or localized gravity processes.

2002–2005 and 2009–2011 Leveling Data Inversion

This study is aimed at comparing the features of the plumbing system active during the 2000s with those retrieved for the present unrest. We consider the literature leveling data related to the 2002–2005 unrest and successive 2009–2011 subsidence (data redrawn from Xu et al., 2012). The 2002–2005 unrest shows a maximum of 6.5 cm uplift close to the caldera along the North route (levelling routes shown in **Figure 2**). Since 2006, the ground uplifted at a slower rate until 2009, when a subsidence phase started. For the subsidence phase we consider elevation changes from North and West leveling routes, amounting to -8 mm maximum close to the caldera.

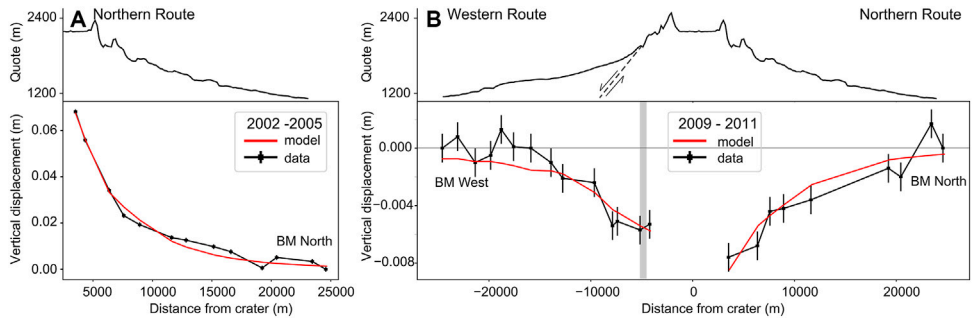

FIGURE 4 | (A) Elevation changes along the northern leveling route during the 2002–2005 unrest and **(B)** height changes along the northern and western routes during the subsidence 2009–2011 (leveling routes reported in **Figure 2**). The vertical bars on data points are the uncertainty associated with the leveling data. The grey vertical bar is the approximate location of the NW-SE trending fault trace located in the western flank of the volcano. Leveling data redrawn from Xu et al. (2012). On the top is reported the topographic profile along the leveling routes. The dashed line is the NW-SE fault seen in a section across the volcano edifice.

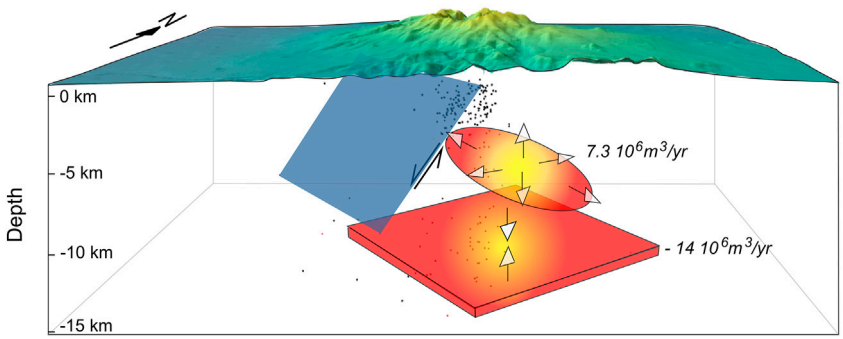

FIGURE 5 | Schematic of the sources of deformation at Changbaishan volcano. The plot is in scale, with double elevation for the topography. The seismicity between 2002–2006 is reported with black dots.

The Bayesian inversions are performed using the above mentioned VSM tool. To limit the number of unknown parameters due to the few available benchmarks, we consider only part of the deformation sources investigated above. The 2002–2005 leveling data consist of the North levelling route alone; therefore we consider only a simplified isotropic point-source (Mogi, 1958). The horizontal position of the isotropic point-source is kept equal to that obtained for the spheroidal source, while its depth and volume variation may vary. Since the 2009–2011 data account for the western sector also, we include the NW-SE fault with parameters fixed as for the inversion of the InSAR data (**Supplementary Table S1**). Results of the leveling data inversions are summarized in **Supplementary Table S2** and **Figure 4**.

The uplift during the 2002–2005 unrest is best modelled by a point-source placed at 4.4 km b.s.L., with a volume variation of $14 \times 106\ m^3$ accumulated in 3 years, i.e., an annual rate of $4.7 \times 106\ m^3$/yr. The source is shallower than that retrieved by ALOS-2 data and its volume variation annual rate is less than that obtained with ALOS-2 data. For the 2009–2011 subsidence, we retrieve a point-source at 6.7 km b.s.L., slightly shallower than that retrieved by InSAR. The annual contraction amounts to -1.4 $\times$ $106\ m^3$/yr, a small fraction of that retrieved for the spheroid depicted by InSAR. The NW-SE fault undergoes a dip-slip of about 1 mm/yr, a value much smaller than that retrieved by InSAR. These values may be considered indicative because of the limited resolving power of the few leveling measurements.

DISCUSSION

The 2018–2020 Deformation Phase

A sketch of the retrieved sources at Changbaishan is reported in **Figure 5**. The results of our analysis of the 2018–2020 ALOS-2 data show that Changbaishan is affected by a general uplift of its southeastern flank with values up to 20 mm/yr and by a significant subsidence, down to –20 mm/yr of its southwestern sector at altitudes less than about 2000 m. The uplift zone is NW-SE elongated and mainly extends in the North Korea sector of the edifice, where the maximum deformation is recorded. A similar deformation field has been detected by Chen et al. (2008) in 2002 and 2003 from the analysis of ENVISAT SAR and JERS-1 SAR data. The maximum elongation of the 2018–2020 uplifting area detected by our analysis follows the Baishan-Jianchi fault regional fault system. Also, the results of our modeling indicate that the NW-SE striking fault affecting the western flank of the volcano

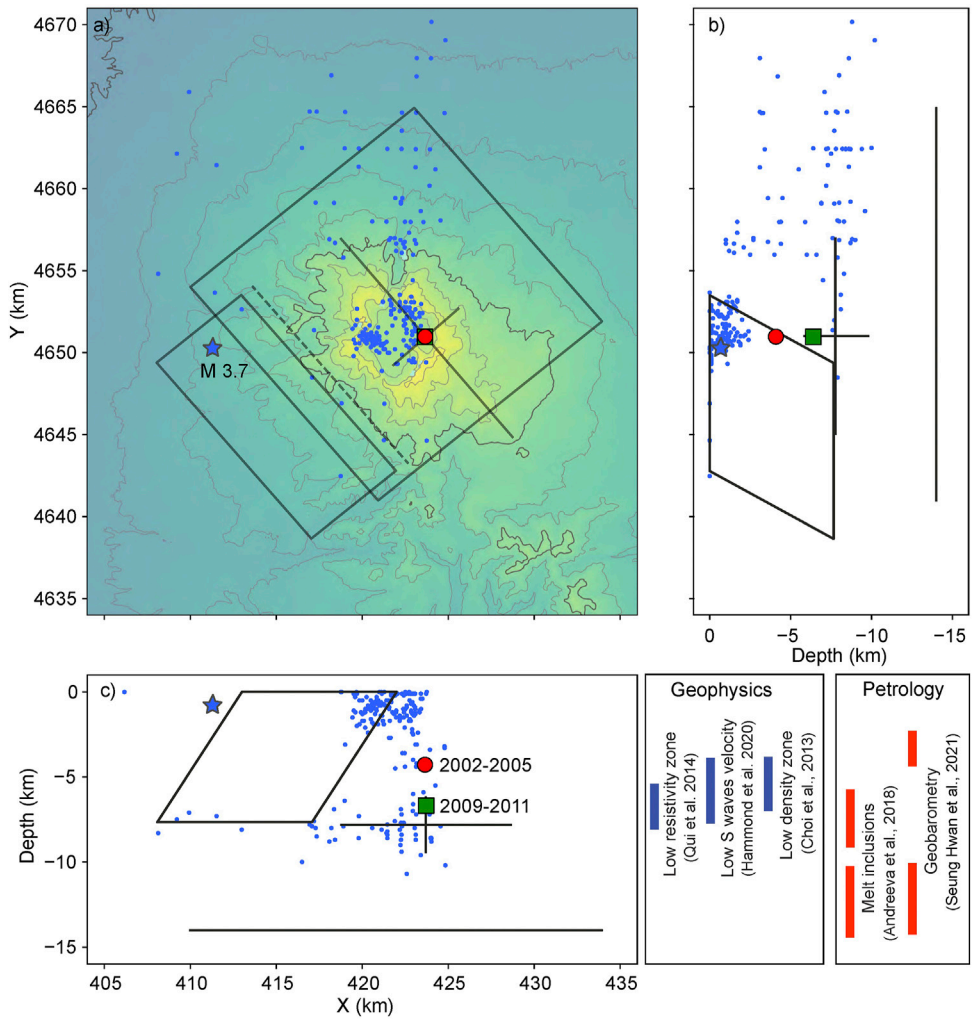

FIGURE 6 | 3D view of seismicity during 2002–2006 (blue dots, the star is the M 3.7 of October 22, 2006) and the active deformation system at Changbaishan at different epochs; **(A)** plane view, **(B)** depth vs North coordinate, and **(C)** East coordinate vs depth. In dark grey are reported the sources retrieved by ALOS2 data for 2018–2020. The spheroid is indicated with its axes. The red circle is the location of the 2002–2006 source, while the location of the 2009–2011 is reported with green square. UTM-WGS84 Zone 52N used as projected coordinates. Topography contour in **(A)** every 200 m, with bold line at 1,000 m. The inferred depth of magma storage zones from available geophysical and petrological data are reported in the bottom right insets.

separates the zone of uplift from that of subsidence. The occurrence of past earthquakes along this discontinuity (**Figure 1**) and our deformation data reveal that this fault is active and moves by creep with normal mechanism and slip-rate of 0.019 m/yr during 2018–2020. This slip-rate corresponds to a geodetic scalar moment in the order of 10^{15} Nm/yr, equivalent to the energy released by a Mw = 3.9 earthquake (Kanamori, 1977). The creep movement of faults during the inflation/deflation phases is not peculiar to Changbaishan but has been detected at other volcanoes, e.g. at Campi Flegrei (Vilardo et al., 2010), Etna (Bonforte et al., 2007) and Ischia (Trasatti et al., 2019), Italy.

At Changbaishan, the evidence of the 2018–2020 NW-SE elongated nearly-inflation and normal fault-like pattern suggests that the deformation field is possibly controlled by the NW-SE striking Baishan-Jianchi fault system (**Figure 1**). According to Zhang et al. (2018), most of the monogenetic cones concentrate along this fault system, suggesting that it represents a preferential path for magma ascent (**Figure 1B**). Our results of the modeling of the recorded uplift suggest that a tabular, deflating deep source at 14 km b.s.L. decreases its volume at a rate of about −14,106 m^3/yr, while the NW-SE elongated, shallower source at 7–8 km depth inflates at a rate of 7.3 106 m^3/yr (**Supplementary Table S1**). The geometry and depth of such sources are consistent with the results from petrological data (Andreeva et al., 2018; Yi et al., 2021; Lee et al., 2021) and gravity modeling (Choi et al., 2013), which show that the Changbaishan plumbing system consists of magma reservoirs with tabular or sill-like geometry located at different depths. Andreeva et al. (2018), Lee et al. (2021) and Choi et al. (2013) suggest the presence of a deep reservoir at about 10–15 km depth in which basaltic melts easily accumulate and upraise to a shallower, from 8 km to about 5.5 km deep reservoir where

magma may evolve to form basaltic trachyandesites and trachytes. The low number of earthquakes below 10 km depth and between 3 and 7 km depth (Liu et al., 2021) supports the hypothesis of the occurrence of such magma reservoirs at these depths (**Figure 6**). Receiver function (Hammond et al., 2020) and magnetotelluric data (Qiu et al., 2014) also reveal a reduction of seismic velocities and a low resistivity zone between 4 and 8 km depth, suggesting the occurrence of melt. Considering these independent estimates regarding the depth and geometry of the Changbaishan magma reservoirs, we conclude that the tabular and deflating source at 14 km depth evidenced by our modeling of the ALOS-2 data is compatible with the 10–15 km deep basaltic reservoir. Also, the shallower, inflating spheroidal reservoir at 7.7 km b.s.L. may correspond to the 4–8 km deep basaltic trachyandesitic to trachytic magma chamber. Then, the NW-SE elongation of the spheroid reflects the tectonic setting of the region since the magma storage takes place in optimal stress orientation regime. Therefore, the 2018–2020 deformation field records a transfer of magma from a deeper to a shallower source, a mechanism observed at other volcanoes, e.g. at Grímsvötn, Iceland (Reverso et al., 2014).

Here, we consider the inferred volumetric changes deduced for the two reservoirs and use their difference to determine the bulk modulus of the magma in the reservoir. The relation linking the volume change of a spherical magma chamber ΔV_c and the magma flow ΔV_m into/out is (Johnson, 1992; Johnson et al., 2000; Hautmann et al., 2017):

$$\Delta V_m = \frac{2}{3}\left(\frac{4\mu}{3K}\right)\Delta V_c$$

with μ as the crustal shear modulus and K as the bulk modulus of the magma. By using $|\Delta V_c| = 14 \times 106\ m^3/yr$ and $\Delta V_m = 7.3 \times 106\ m^3/yr$ (**Supplementary Table S1**) and adopting an average crustal shear modulus of 30 GPa, we determine a magma bulk modulus of 51 GPa, a value consistent with that of basaltic melts (K = 50–60 GPa between 1,000 and 1,200°C; Schilling et al., 2003). This should be considered in terms of order of magnitude estimate because of the spherical geometry assumption. Considering this result, the volume deficit observed in the transfer of magma from the deflating and deeper reservoir to the shallower one cannot be attributed to magma compressibility (=1/K), i.e. magma plus gas. Therefore, we suggest, according to the crystal-mush model proposed by Yi et al. (2021) for the plumbing system of Changbaishan, that about half of the gas-poor melt volume exiting from the 14 km deep reservoir intrudes a porous crystal-mush, while the remaining half enters the 7.7 km deep sill-like reservoir. The conduit separating the two reservoirs has a vertical length of about 6.3 km. By ignoring horizontal extensional stresses and assuming an overpressure P_f = 10 MPa (Manga and Brodsky, 2006), the width a of a dike-like conduit may be calculated by the relation (Hartley and Maclennan, 2018):

$$a = hP_f/\mu$$

by selecting μ = 30 GPa and h = 6.3 km, we obtain $a \sim 2$ m. The vertically directed upward force on the magma column between the two reservoirs is given by $\Delta\rho gh$, with $\Delta\rho$ the density difference between magma and host rocks, g the gravity acceleration and h the difference between the depths of the two reservoirs. Assuming $\Delta\rho$ between 100 and 200 kg/m^3, the vertically directed upward force on the column is about 13–27 MPa, a value larger than the 1–10 MPa pressure required for basaltic reservoirs to open a crack so allowing magma uprising (Manga and Brodsky, 2006). We underline that the volume variation of the conduit amounts to $2 \times 104\ m^3$, that is 2-3 orders of magnitude less than the volume variation of the two reservoirs, and therefore it is not constrainable by geodetic data.

The 2002–2005 Uplift and 2009–2011 Subsidence Phases

Our results from the inversion of levelling data (Xu et al., 2012) relative to the 2002–2005 uplift during the unrest phase and the 2009–2011 subsidence consist in:

1) a point-source inflating between 2002 and 2005 with a volume variation rate of $4.6 \times 106\ m^3/yr$ and depth 4.4 km b.s.l. As previously reported, the source is shallower than that retrieved by ALOS-2 data and the annual rate of volume variations is also less than that recorded for the 2018–2020 period. This is due to the shallower depth retrieved for the 2002–2005 source. Both the 2002–2005 point-source and the 2018–2020 spheroid are coaxial.
2) A point-source deflating at a rate of $-1.4 \times 106\ m^3/yr$ at 6.7 km b.s.L. is inferred for the 2009–2011 period. Also, the NW-SE striking fault affecting the western flank of the volcano fault shows a slip-rate of about 1 mm/yr, a rate smaller than that inferred for the 2018–2020 inflation. Also in this case, both the point-source and the spheroid of 2018–2020 are coaxial.

The above summarized values must be considered in terms of their order of magnitude, because, according to Ji et al. (2021), the limited distribution of the geodetic sites on the northern and western sides of the volcano does not allow us to constrain the whole deformation pattern of Changbaishan. However, some inferences on the processes occurred during the uplift and the following subsidence phase may be suggested. The increase in CO_2 concentration and values of the He isotopic ratio (Xu et al., 2012) in the emitted gases during the uplift indicate the involvement of a pressurized degassing magmatic source possibly located, according to our modeling results, at 4.4 km depth (**Figure 6**). This conclusion is supported by the lack of earthquakes at this depth during 2002–2006 (Liu et al., 2021). While the 2002–2006 uplift mainly recorded the arrival of gas to the top of the reservoir, the successive 2009–2011 subsidence, whose source is about 2 km deeper than of the uplift, can be associated to gas release and crystallization processes in the middle/lower portions of the reservoir. This mechanism has been proposed to explain the deflation following previous uplift phases associated with unrest episodes at other volcanoes, e.g., at Okmok volcano, Aleutians (Caricchi et al., 2014) and Santorini, Greece (Papageorgiou et al., 2019).

Following this mechanism, the difference in depth between the sources responsible for the 2002–2005 uplift and 2009–2011 subsidence at Changbaishan does not imply the occurrence of two separated reservoirs but a single, vertically extended magma chamber affected by an early magma intrusion and pressurized degassing and by a later crystallization associated to passive gas release. Both the source depths retrieved for the 2002–2005 uplift and 2009–2011 subsidence are consistent with the 4–8 km deep basaltic trachyandesitic to trachytic magma chamber as discussed above for the 2018–2020. The depth of the point-source related to the subsidence is consistent with that determined for the shallower reservoir related to the 2018–2020 uplift (**Supplementary Tables S1, S2**).

Magma Recharge and Implications for the Monitoring

Our results highlight that the Changbaishan magmatic system is still active and consists of reservoirs located at different depths whose present-day dynamics is associated with recharge processes, a feature consistent with the available petrological and geochemical data on past eruptions (Zhang et al., 2018; Yi et al., 2021) and geophysical data (Choi et al., 2013; Qiu et al., 2014; Hammond et al., 2020). A new upraise of magma may alter a part or the whole plumbing system and potentially trigger an eruption. The ALOS-2 data and related modeling results allow us to suppose the mechanisms of the present-day magma dynamics. Also, the successful exploitation of remote sensing data demonstrates their usefulness in case of under-monitored or partially monitored volcanoes. Because our data recorded a 2018–2020 deformation concentrated on the North Korea sector of the volcano, it may be that the *in-situ* monitoring system located on China territory does not detect the full pattern of signals related to the volcano dynamics. This prevents possible inferences and the correct interpretation of such signals, reducing the ability to properly evaluate the hazard and the efficiency of early warning systems.

CONCLUSION

The results of this study may be summarized in the following main points:

- During 2018–2020 Changbaishan has been characterized by an uplift phase with maximum velocity of 15–20 mm/yr. The uplifted area is NW-SE elongated and mainly affects the North Korea side of the volcano. A NW-SE striking fault affecting the western flank slipped aseismically by creep and accounts for the down to −20 mm/yr subsidence observed in the western plain surrounding the edifice.
- The inversion of the ALOS-2 data identifies two sources of deformation related to magma dynamics. The constrained active plumbing system consists of a deeper (14 km b.s.L.), deflating and tabular source, and a shallower (7.7 km b.s.L.), spheroidal and NW-SE elongated inflating source. The geometry of this latter is confined by the major, NW-SE striking fault system crossing the volcano. The depth of these reservoirs is consistent with independent geophysical and petrological data.
- Our modeling supports the hypothesis of magma transfer from the deeper to the shallow source with a vertically directed upward force of about 13–27 MPa. The width of the dike connecting the two sources is about 2 m. The difference in volume variation between the tabular source and the spheroid evidences that not all the melt from the deeper reservoir is transferred to the shallower one and a part intrudes the crystal-mush plumbing system of the volcano.
- The 2002–2005 uplift and the 2009–2011 subsidence can be explained by two point-sources located at 4.4 and 6.7 km depth, respectively. However, these sources do not mirror two separated reservoirs but a single reservoir whose dynamics reflects an early, 2002–2005 pressurized degassing process associated with the arrival of fresh magma and a later, passive degassing processes coupled to crystallization. Therefore, the uplift is mainly related to the dynamics of the upper portion of the magma chamber, whereas the subsidence is more consistent with the post-emplacement dynamics of its floor. The latter has been reactivated by the arrival of new magma in 2018–2020.

The plumbing system of the Changbaishan volcano is still active, vertically extended and affected by magma recharging processes at different depths. A monitoring system including massive analysis of satellite data will ensure a full spatial coverage of the deformation field at the China/North Korea border associated with possible pre-eruptive unrests.

DATA AVAILABILITY STATEMENT

The mean ground velocity data can be found at https://reliance.rohub.org/overview?61bceafe-5b48-4548-8caf-4142153b1b1b, with doi: https://doi.org/10.24424/vfp6-r230. Raw data is property of JAXA.

AUTHOR CONTRIBUTIONS

Conceptualization, GV, ET, and CT; Formal analysis, ET, CT, and LW; Writing, all; Validation, LW; Investigation, GV. All authors have read and agreed to the published version of the manuscript.

FUNDING

This study has been funded by the Natural Science Foundation of China (grant no. 42071453), the Fundamental Research Funds for Central Universities (grant no. N2001027) and the cooperation project "Dragon 5" (grant no. 58029) between European Space Agency (ESA) and Ministry of Science and Technology (MOST) of the P.R. China. It has been partially supported by Pianeta

Dinamico—Working Earth, a project between the Italian Ministry of University and Research and INGV.

ACKNOWLEDGMENTS

ALOS-2 data were obtained for courtesy of the JAXA agency in the framework of the Earth Observations Collaborative Research Agreement between the Japanese Aerospace Exploration Agency and the Research Organization (No. ER2A2N173A). We thank Guoming Liu of the Changbaishan Volcano Observatory (Institute of Volcanology, CEA), Xuanlong Shan (Jilin University), and Zhengfu Guo (Institute of Geology and Geophysics, CAS) for the constructive exchanges on the issues related to the Changbaishan volcanism and the topics discussed in this work. We thank Marco Polcari (INGV) for cross-checking the InSAR data processing.

SUPPLEMENTARY MATERIAL

The Supplementary Material for this article can be found online at: https://www.frontiersin.org/articles/10.3389/feart.2021.741287/full#supplementary-material

REFERENCES

Acocella, V., Di Lorenzo, R., Newhall, C., and Scandone, R. (2015). An Overview of Recent (1988 to 2014) Caldera Unrest: Knowledge and Perspectives. *Rev. Geophys.* 53, 896–955. doi:10.1002/2015RG000492

Andreeva, O. A., Yarmolyuk, V. V., Andreeva, I. A., and Borisovskiy, S. E. (2018). Magmatic Evolution of Changbaishan Tianchi Volcano, China–North Korea: Evidence From Mineral-Hosted Melt and Fluid Inclusions. *Petrology.* 26, 515–545. doi:10.1134/s0869591118050028

Berardino, P., Fornaro, G., Lanari, R., and Sansosti, E. (2002). A New Algorithm for Surface Deformation Monitoring Based on Small Baseline Differential SAR Interferograms. *IEEE Trans. Geosci. Remote Sensing.* 40, 2375–2383. doi:10.1109/tgrs.2002.803792

Bonaccorso, A., Cianetti, S., Giunchi, C., Trasatti, E., Bonafede, M., and Boschi, E. (2005). Analytical and 3-D Numerical Modelling of Mt. Etna (Italy) Volcano Inflation. *Geophys. J. Int.* 163, 852–862. doi:10.1111/j.1365-246X.2005.02777.x

Bonforte, A., Branca, S., and Palano, M. (2007). Geometric and Kinematic Variations Along the Active Pernicana Fault: Implication for the Dynamics of Mount Etna NE Flank (Italy). *J. Volcanol. Geotherm. Res.* 160 (1-2), 210–222. doi:10.1016/j.jvolgeores.2006.08.009

Caricchi, L., Biggs, J., Annen, C., and Ebmeier, S. (2014). The Influence of Cooling, Crystallisation and Re-melting on the Interpretation of Geodetic Signals in Volcanic Systems. *Earth Planet. Sci. Lett.* 388, 166–174. doi:10.1016/j.epsl.2013.12.002

Casu, F., Manzo, M., and Lanari, R. (2006). A Quantitative Assessment of the SBAS Algorithm Performance for Surface Deformation Retrieval From DInSAR Data. *Remote Sensing Environ.* 102, 195–210. doi:10.1016/j.rse.2006.01.023

Chang, W.-L., Smith, R. B., Farrell, J., and Puskas, C. M. (2010). An Extraordinary Episode of Yellowstone Caldera Uplift, 2004-2010, From GPS and InSAR Observations. *Geophys. Res. Lett.* 37, a–n. doi:10.1029/2010GL045451

Chen, G.-H., Shan, X.-J., Moon, W. M., and Kim, K.-R. (2008). A modeling of the Magma Chamber Beneath the Changbai Mountains Volcanic Area Constrained by InSAR and GPS Derived Deformation. *Chin. J. Geophys.* 51, 765–773. doi:10.1002/cjg2.1269

Choi, S., Oh, C.-W., and Götze, H.-J. (2013). Three-Dimensional Density Modeling of the EGM2008 Gravity Field over the Mount Paekdu Volcanic Area. *J. Geophys. Res. Solid Earth.* 118, 3820–3836. doi:10.1002/jgrb.50266

Farr, T. G., Rosen, P. A., Caro, E., Crippen, R., Duren, R., Hensley, S., et al. (2007). The Shuttle Radar Topography Mission. *Rev. Geophys.* 45, RG2004. doi:10.1029/2005RG000183

Ferretti, A., Prati, C., and Rocca, F. (2001). Permanent Scatterers in SAR Interferometry. *IEEE Trans. Geosci. Remote Sensing.* 39, 8–20. doi:10.1109/36.898661

Hamling, I. J., Hreinsdóttir, S., Bannister, S., and Palmer, N. (2016). Off-Axis Magmatism Along a Subaerial Back-Arc Rift: Observations From the Taupo Volcanic Zone, New Zealand. *Sci. Adv.* 2 (6), e1600288. doi:10.1126/sciadv.1600288

Hammond, J. O. S., Wu, J.-P., Ri, K.-S., Wei, W., Yu, J.-N., and Oppenheimer, C. (2020). Distribution of Partial Melt Beneath Changbaishan/Paektu Volcano, China/Democratic People's Republic of Korea. *Geochem. Geophys. Geosys.* 21, e2019GC008461. doi:10.1029/2019gc008461

Hartley, M., and Maclennan, J. (2018). Magmatic Densities Control Erupted Volumes in Icelandic Volcanic Systems. *Front. Earth Sci.Earth Sci.* 6, 29. doi:10.3389/feart.2018.00029

Hautmann, S., Sacks, I. S., Linde, A. T., and Roberts, M. J. (2017). Magma Buoyancy and Volatile Ascent Driving Autocyclic Eruptivity at Hekla Volcano (Iceland). *Geochem. Geophys. Geosyst.* 18, 3517–3529. doi:10.1002/2017GC007061

Horn, S., and Schmincke, H.-U. (2000). Volatile Emission During the Eruption of Baitoushan Volcano (China/North Korea) Ca. 969 AD. *Bull. Volcanol.* 61, 537–555. doi:10.1007/s004450050004

Iacovino, K., Ju-Song, K., Sisson, T., Lowenstern, J., Kuk-Hun, R., Jong-Nam, J., et al. (2016). Quantifying Gas Emissions from the "Millennium Eruption" of Paektu Volcano, Democratic People's Republic of Korea/China. *Sci. Adv.* 2, 11e1600913. doi:10.1126/sciadv.1600913

Ji, L., Xu, J., Lin, X., and Luan, P. (2010). Application of Satellite Thermal Infrared Remote Sensing in Monitoring Magmatic Activity of Changbaishan Tianchi Volcano. *Chin. Sci. Bull.* 55 (24), 2731–2737. doi:10.1007/s11434-010-3232-2

Ji, L., Xu, J., Liu, L., and Zhang, W. (2021). A Review of Present-Day Deformation of Active Volcanoes in China Between 1970 and 2013. *Geol. Soc. Lond. Spec. Publications.* 510, 215–226. doi:10.1144/SP510-2019-228

Ji, L., Xu, J., Wang, Q., and Wan, Y. (2013). Episodic Deformation at Changbaishan Tianchi Volcano, Northeast China during 2004 to 2010, Observed by Persistent Scatterer Interferometric Synthetic Aperture Radar. *J. Appl. Remote Sens.* 7, 073499–73499. doi:10.1117/1.JRS.7.073499

Johnson, D. J. (1992). Dynamics of Magma Storage in the Summit Reservoir of Kilauea Volcano, Hawaii. *J. Geophys. Res.* 97, 1807–1820. doi:10.1029/91jb02839

Johnson, D. J., Sigmundsson, F., and Delaney, P. T. (2000). Comment on " Volume of Magma Accumulation or Withdrawal Estimated From Surface Uplift or Subsidence, with Application to the 1960 Collapse of Kīlauea Volcano" by P. T. Delaney and D. F. McTigue. *Bull. Volcanology.* 61, 491–493. doi:10.1007/s004450050006

Kanamori, H. (1977). The Energy Release in Great Earthquakes. *J. Geophys. Res.* 82 (20), 2981–2987. doi:10.1029/jb082i020p02981

Kennedy, B. M., Holohan, E. P., Stix, J., Gravley, J. R. J., and Cole, J. W. (2018). Magma Plumbing Beneath Collapse Caldera Volcanic Systems. *Earth-Science Rev.* 177, 404–424. doi:10.1016/j.earscirev.2017.12.002

Lee, S. H., Oh, C. W., Lee, Y. S., Lee, S.-G., and Liu, J.-q. (2021). Petrogenesis of the Cenozoic Volcanic Rocks in Baekdu Volcano in Northeastern Asia and the Expected Depth of the Magma Chamber Based on Geochemistry, Mineral Chemistry, and Sr-Nd-Pb Isotope Chemistry. *Lithos.* 388-389, 106080. doi:10.1016/j.lithos.2021.106080

Liu, G., Li, C., Peng, Z., Liu, Y., Zhang, Y., Liu, D., et al. (2021). The 2002-2005 Changbaishan Volcanic Unrest Triggered by the 2002 M 7.2 Wangqing Deep Focus Earthquake. *Front. Earth Sci.* 8, 599329. doi:10.3389/feart.2020.599329

Liu, M., Gu, M., Sun, Z., Wei, H., and Jin, B. (2004). Activity of Main Faults and Hydrothermal Alteration Zone at the Tianchi Volcano, Changbaishan. *Earthq. Res. China.* 20 (10), 64–72. (in Chinese).

Manga, M., and Brodsky, E. (2006). Seismic Triggering of Eruptions in the Far Field: Volcanoes and Geysers. *Annu. Rev. Earth Planet. Sci.* 34, 263–291. doi:10.1146/annurev.earth.34.031405.125125

Mogi, K. (1958). Relations Between Eruptions of Various Volcanoes and the Deformations of the Ground Surfaces Around Them. *Bull. Earthq. Res. Inst. Tokyo Univ.* 36, 99.

Mosegaard, K., and Tarantola, A. (1995). Monte Carlo Sampling of Solutions to Inverse Problems. *J. Geophys. Res.* 100 (B7), 12 431–512 447. doi:10.1029/94jb03097

Newhall, C. G., and Dzurisin, D. (1988). *Historical Unrest at Large Calderas of the World*. Reston, VA: US Geological Survey Bulletin n, 1855.

Okada, Y. (1985). Surface Deformation Due to Shear and Tensile Faults in a Half-Space. *Bull. Seismol. Soc. Am.* 75, 1135–1154. doi:10.1785/bssa0750041135

Pan, B., Liu, G., Cheng, T., Zhang, J., Sun, Z., Ma, B., et al. (2021). Development and Status of Active Volcano monitoring in China. *Geol. Soc. Lond. Spec. Publications.* 510, 227–252. doi:10.1144/SP510-2020-62

Papageorgiou, E., Foumelis, M., Trasatti, E., Ventura, G., Raucoules, D., and Mouratidis, A. (2019). Multi-Sensor SAR Geodetic Imaging and Modelling of Santorini Volcano Post-Unrest Response. *Remote Sensing.* 11 (3), 259. doi:10.3390/rs11030259

Parker, A. L., Biggs, J., Walters, R. J., Ebmeier, S. K., Wright, T. J., Teanby, N. A., et al. (2015). Systematic Assessment of Atmospheric Uncertainties for InSAR Data at Volcanic Arcs Using Large-Scale Atmospheric Models: Application to the Cascade Volcanoes, United States. *Remote Sensing Environ.* 170, 102–114. doi:10.1016/j.rse.2015.09.003

Peltzer, G., and Rosen, P. (1995). Surface Displacement of the 17 May 1993 Eureka Valley, California, Earthquake Observed by SAR Interferometry. *Science.* 268, 1333–1336. doi:10.1126/science.268.5215.1333

Phillipson, G., Sobradelo, R., and Gottsmann, J. (2013). Global Volcanic Unrest in the 21st Century: An Analysis of the First Decade. *J. Volcanology Geothermal Res.* 264, 183–196. doi:10.1016/j.jvolgeores.2013.08.004

Qiu, G., Pei, F., Fang, H., Du, B., Zhang, X., Zhang, P., et al. (2014). Analysis of Magma Chamber at the Tianchi Volcano Area in Changbai mountain. *Chin. J. Geophys.* 57, 3466–3477. doi:10.6038/cjg20141032

Reverso, T., Vandemeulebrouck, J., Jouanne, F., Pinel, V., Villemin, T., Sturkell, E., et al. (2014). A Two-Magma Chamber Model as a Source of Deformation at Grímsvötn Volcano, Iceland. *J. Geophys. Res. Solid Earth.* 119 (6), 4666–4683. doi:10.1002/2013jb010569

Schilling, F. R., Sinogeikin, S. V., Hauser, M., and Bass, J. D. (2003). Elastic Properties of Model Basaltic Melt Compositions at High Temperatures. *J. Geophys. Res.* 108 (B6), 2304. doi:10.1029/2001JB000517

Sturkell, E., Ágústsson, K., Linde, A. T., Sacks, S. I., Einarsson, P., Sigmundsson, F., et al. (2013). New Insights into Volcanic Activity From Strain and Other Deformation Data for the Hekla 2000 Eruption. *J. Volcanology Geothermal Res.* 256, 78–86. doi:10.1016/j.jvolgeores.2013.02.001

Sun, C., Plunkett, G., Liu, J., Zhao, H., Sigl, M., McConnell, J. R., et al. (2014). Ash From Changbaishan Millennium Eruption Recorded in Greenland Ice: Implications for Determining the Eruption's Timing and Impact. *Geophys. Res. Lett.* 41, 694–701. doi:10.1002/2013GL058642

Trasatti, E., Acocella, V., Di Vito, M. A., Del Gaudio, C., Weber, G., Aquino, I., et al. (2019). Magma Degassing as a Source of Long-Term Seismicity at Volcanoes: The Ischia Island (Italy) Case. *Geophys. Res. Lett.* 46, 14421–14429. doi:10.1029/2019GL085371

Trasatti, E., Polcari, M., Bonafede, M., and Stramondo, S. (2015). Geodetic Constraints to the Source Mechanism of the 2011-2013 Unrest at Campi Flegrei (Italy) Caldera. *Geophys. Res. Lett.* 42, 3847–3854. doi:10.1002/2015GL063621

Trasatti, E. (2019). Volcano and Seismic Source Modeling - VSM. Available at http://www.rohub.org/rodetails/volcano_source_modelling_vsm-release/overview.

Vilardo, G., Isaia, R., Ventura, G., De Martino, P., and Terranova, C. (2010). InSAR Permanent Scatterer Analysis Reveals Fault Re-Activation during Inflation and Deflation Episodes at Campi Flegrei Caldera. *Remote Sensing Environ.* 114, 2373–2383. doi:10.1016/j.rse.2010.05.014

Xu, J., Liu, G., Wu, J., Ming, Y., Wang, Q., Cui, D., et al. (2012). Recent Unrest of Changbaishan Volcano, Northeast China: a Precursor of a Future Eruption? *Geophys. Res. Lett.* 39, a–n. doi:10.1029/2012GL052600

Yang, X.-M., Davis, P. M., and Dieterich, J. H. (1988). Deformation from Inflation of a Dipping Finite Prolate Spheroid in an Elastic Half-Space as a Model for Volcanic Stressing. *J. Geophys. Res.* 93, 4249–4257. doi:10.1029/jb093ib05p04249

Yi, J., Wang, P., Shan, X., Ventura, G., Wu, C., Guo, J., et al. (2021). Modeling the Multi-Level Plumbing System of the Changbaishan Caldera From Geochemical, Mineralogical, Sr-Nd Isotopic and Integrated Geophysical Data. *Geosci. Front.* 12, 101171. doi:10.1016/j.gsf.2021.101171

Zhang, M., Guo, Z., Liu, J., Liu, G., Zhang, L., Zhao, W., et al. (2018). The Intraplate Changbaishan Volcanic Field (China/North Korea): A Review on Eruptive History, Magma Genesis, Geodynamic Significance, Recent Dynamics and Potential Hazards. *Earth-Science Rev.* 187, 19–52. doi:10.1016/j.earscirev.2018.07.011

Zhang, M., Guo, Z., Sano, Y., Cheng, Z., and Zhang, L. (2015). Stagnant Subducted Pacific Slab-Derived CO2 Emissions: Insights Into magma Degassing at Changbaishan Volcano, NE China. *J. Asian Earth Sci.* 106, 49–63. doi:10.1016/j.jseaes.2015.01.029

Zhao, D. (2021). Seismic Imaging of Northwest Pacific and East Asia: New Insight Into Volcanism, Seismogenesis and Geodynamics. *Earth-Science Rev.* 214, 103507. doi:10.1016/j.earscirev.2021.103507

Zhu, G.-Z., Wang, Q.-L., and Cui, D.-X. (2008). Modelling Pressurized Deformation Source for Changbaishan Volcano With Homogenous Expansion Point Source. *Chin. J. Geophys.* 51, 89–96. (in Chinese with English abstract). doi:10.1002/cjg2.1197

Conflict of Interest: The authors declare that the research was conducted in the absence of any commercial or financial relationships that could be construed as a potential conflict of interest.

Publisher's Note: All claims expressed in this article are solely those of the authors and do not necessarily represent those of their affiliated organizations, or those of the publisher, the editors and the reviewers. Any product that may be evaluated in this article, or claim that may be made by its manufacturer, is not guaranteed or endorsed by the publisher.